ChemPubSoc Europe

DOI: 10.1002/open.201900327

Open Access ChemistryOPEN Full Papers

Gas-Sensing Activity of Amorphous Copper Oxide Porous Nanosheets

Zheng Tian,[a, b] Hua Bai,[b] Yahui Li,[b] Wei Liu,[b] Junfang Li,[b] Qinghong Kong,*[a] and Guangcheng Xi*[b]

In this paper, the gas-sensing properties of copper oxide porous nanosheets in amorphous and highly crystalline states were comparatively investigated on the premise of almost the same specific surface area, morphology and size. Unexpectedly, the results show that amorphous copper oxide porous nanosheets have much better gas sensing properties than highly crystalline copper oxide to a serious of volatile organic compounds, and the lowest detection limit (LOD) of the amorphous copper oxide porous nanosheets to methanal is even up to 10 ppb. By contrast, the LOD of the highly crystalline copper oxide porous nanosheets to methanal is 95 ppb. Experiments prove that the oxygen vacancies contained in the amorphous copper oxide porous nanosheets play a key role in improving gas sensitivity, which greatly improve the chemical activity of the materials, especially for the adsorption of molecules containing oxygen-groups such as methanal and oxygen.

1. Introduction

Many toxic volatile organic compounds (VOCs) caused by the interior decoration and new furniture have become a serious threat to the health of residents.[1–3] Among these gaseous pollutants, methanal is one of the most common and most hazardous, because of its slow release process would late for decades.[4–5] methanal gas with a concentration of only 80 ppb may cause human tissue carcinogenesis.[6] Thus, it is necessary to monitor these carcinogenic VOCs. The core of solving these problems is to accurately and quickly detect the existence of these dangerous substances, so it is necessary to develop a high performance gas sensor to fulfil the actual needs. After years of research, the metal oxide-based gas sensors have been given great expectations to resolve the problems of poor detect limit in low gas concentration.[7–10] Recently, several effective methods have been developed to improve the performance of gas sensor, such as the material nanocrystallization,[11–13] the construction of porous structure,[14–16] introducing heteroatoms,[17,18] and the introduction lattice defects.[19,20] It is noted these reported metal oxide-based gas-sensing materials are almost all highly crystalline, and it is unknown whether amorphous metal oxides nanostructures can be used as effective gas sensitive materials. Therefore, it is necessary to make a rigorous comparative study of the gas-sensing properties of the amorphous and crystalline phases of the same metal oxide, which would provide useful clues for the understanding of the gas-sensing mechanism and designing more effective sensing materials. However, the premise for this rigorous comparative study is that we can produce amorphous and crystalline materials with the almost same component, specific surface area, and morphology, which is very difficult to achieve this.

As a common metal oxide, p-type semiconductor copper oxide (CuO) with a narrow band gap (1.2 eV) is more and more widely used in the field of gas sensing due to its advantage of low cost, facile synthesis, high reproducibility and nontoxicity.[21] Up to present, crystalline CuO (c-CuO) nanoparticles, nanorods, nanowires, nanobelts and three-dimensional hierarchical porous structures have been successfully synthesized.[22–25] Among them, hierarchically porous structured CuO nanostructures displayed excellent gas sensing properties due to its large specific surface area and abundant accessible pores,[26,27] which could increase the adsorption and desorption of target gas molecules. Besides, several research groups have been demonstrated that the lattice defect will also have a positive effect in the process of gas test.[19,20] These reports inspire us to make a rational hypothesis: whether the amorphous CuO (a-CuO) hierarchical porous structure with a large number of defects will have better gas sensing properties?

Herein, we have successfully synthesized two kinds of well-defined copper oxide hierarchical porous micro/nanostructures, which are all composed of porous nanosheets. Specifically, one is highly crystalline c-CuO, and the other is a-CuO. It is particularly necessary to propose that these two copper oxide nanosheets with totally different crystallinity have almost the same morphology, size and specific surface area. Comparative studies revealed that these a-CuO porous nanosheets exhibit much higher gas sensitivity than the c-CuO porous nanosheets. A variety of characterization methods show that a large number of oxygen-vacancy defects (Vo) exist in a-CuO nanosheets. First-principles density-functional theory calculation reveals that the

[a] Z. Tian, Prof. Q. Kong
School of the Environment and Safety engineering, Jiangsu University, Zhenjiang, 212013, P. R. China
E-mail: kongqh@mail.ujs.edu.cn
[b] Z. Tian, Prof. H. Bai, Y. Li, Dr. W. Liu, Dr. J. Li, Prof. G. Xi
Institute of Industrial and Consumer Product Safety
Chinese Academy of Inspection and Quarantine
No. 11, Ronghua South Road, Beijing
E-mail: xiguangcheng@caiq.org.cn

introduction of Vo can greatly increase the adsorption energies of oxygen and methanal molecules on the surface of the a-CuO porous nanosheet, which also has been demonstrated by chemical adsorption experiments. In addition, the designed hierarchical porous a-CuO microspheres composed of porous nanosheets not only afford an ideal multichannel cavity to realize the gas diffusing in the inner microspheres, but also provide huge surface areas for the efficient adsorption of probe molecules. To the best of our knowledge, this is the first time to clearly observe the remarkable gas-sending activity from amorphous semiconductor materials, which may open a new frontier for highly sensitive and stable sensing technology.

2. Results and Discussion

2.1. Design of Synthetic Route

To obtain amorphous a-CuO and highly crystalline c-CuO porous nanosheets respectively, two synthetic routes were reasonably designed. As shown in Scheme 1, whether it is for the synthesis of a-CuO or c-CuO porous nanosheets, the first step is the preparation of $Cu_2(OH)_2CO_3$ precursor; next, by heating the $Cu_2(OH)_2CO_3$ is decomposed into CuO, H_2O and CO_2. We designed two heating decomposition routes, one is the fast high-power microwave-heating route, it is expected that this rapid heating can produce crystal phase transition far from equilibrium state, generating amorphous a-CuO porous nanosheets; while the other one we selected is the slow annealing process, it is expected that the crystalline phase transition process of the nearly equilibrium state can produce highly crystallized c-CuO porous nanosheets. It should be noted that the no harmful substances were produced in the synthetic xperiments, and the precursors were very common and cheap, so it shows the environment friendly characteristic and high operability of the method.

2.2. Structure and Morphology Characterization of a-CuO and c-CuO Porous Nanosheets

By a hydrothermal hydrolysis process in the first step, a green and fluffy product was first synthesized. X-ray diffraction (XRD) pattern shows that the green product is $Cu_2(OH)_2CO_3$ (JCPDS. 56-0001, black pattern in Figure S2). This green sample is then decomposed into black CuO in two ways: rapid microwave heating and slow heating in the air. On the one hand, XRD pattern revealed that the product generated by slow heating in air is highly crystalline, all the diffraction peaks can be precisely indexed into the monoclinic phase CuO (JCPDS, 48-1548, space group: C2/c) with the lattice parameters of a = 4.688 Å, b = 3.422 Å, and c = 5.1319 Å (red pattern in Figure S2). No diffraction peaks of other crystalline substances were detected. On the other hand, XRD pattern revealed that the black product obtained by rapid microwave heating is amorphous (blue pattern in Figure S2). Elemental analysis showed that the sample was essentially free of carbon and water, and EDS also proved that the two samples contained only Cu and O (Figure S3). The characterization results indicate that $Cu_2(OH)_2CO_3$ has been completely decomposed into amorphous a-CuO and crystalline c-CuO by rapid microwave heating and slow heating in air, respectively.

Furthermore, the morphology and structure of the prepared $Cu_2(OH)_2CO_3$ and CuO samples were investigated by using field-emission scanning electron microscope (FSEM) and transmission electron microscope (TEM). The results from the low-magnification FSEM images of $Cu_2(OH)_2CO_3$ (Figure S4) manifest that the particles synthesized by the hydrothermal method were self-assembled hierarchical microspheres organized by a large number of primary nanosheets and they grew in a radial way from inside to outside. In addition, the high-magnification FSEM images (insert images in Figure S4) illustrate the surfaces of $Cu_2(OH)_2CO_3$ nanosheets were smooth without any pores. After heat treatment, although the microsphere structure remains unchanged (Figure 1a–c), dramatic evidences from Figure 1b–d suggest that the CuO nanosheets generated dense pores and the pore sizes were around 15–30 nm. According to the current research achievements in gas sensor field, the hierarchical structure and porous structure will effectively enhance the specific surface area of the material, facilitate the transmission of target gas, and accelerate the rate of gas response. At the same time, the TEM images also confirmed the hierarchical porous structure of the samples (Figure 2a–d). Although very

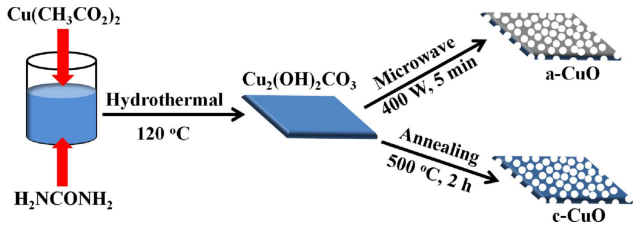

Scheme 1. The designed synthetic route of the c-CuO and a-CuO porous nanosheets.

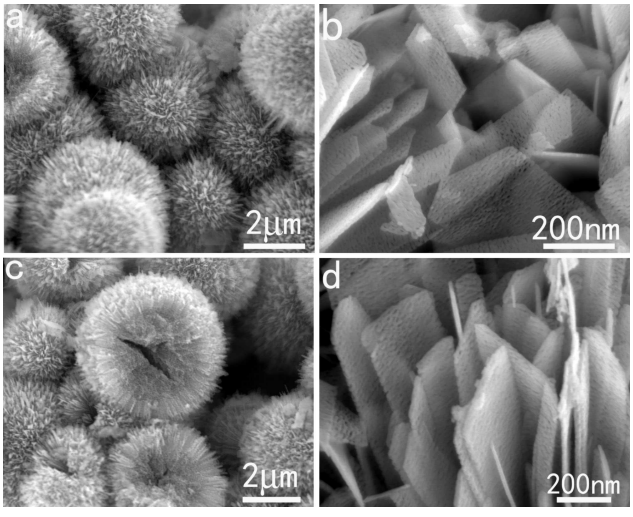

Figure 1. FSEM images of the as-synthesized a-CuO (a–b) and c-CuO porous nanosheets (c–d).

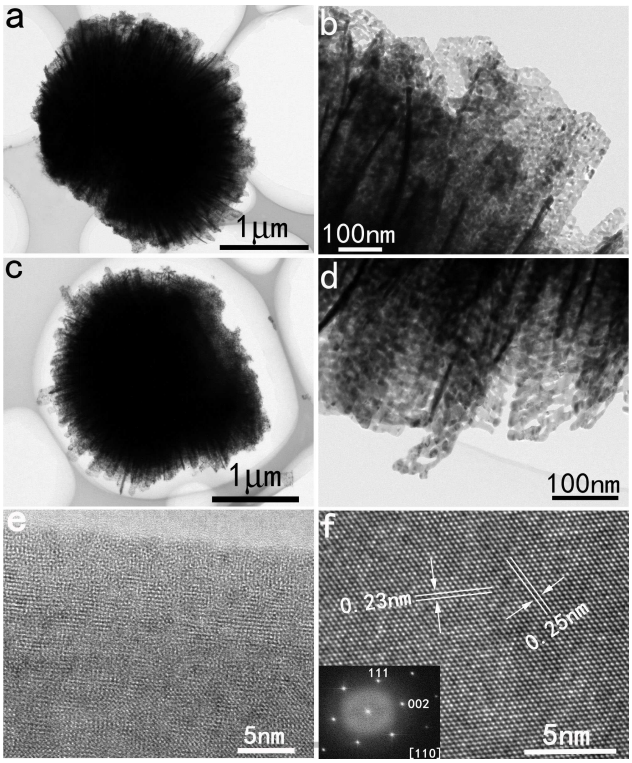

Figure 2. (a–b) TEM images of the a-CuO porous nanosheets. (c–d) TEM images of the c-CuO porous nanosheets. (e) HRTEM image of the a-CuO porous nanosheets. (f) HRTEM image of the c-CuO porous nanosheets.

similar in appearance, the HRTEM images revealed the natural differences in microscopic features of the CuO nanosheets prepared by different synthetic methods. As is shown in Figure 2e, the a-CuO porous nanosheets obtained by microwave-heating have no distinct lattice fringe, which state that the acute and rapid synthetic reaction caused many defects on the body of the material. On the contrary, the c-CuO porous nanosheets generated by slowly heating in air possess a high degree of crystallinity and the spacing of the lattice fringe of 0.25 and 0.23 nm, which correspond to the (002) and (111) planes of monoclinic CuO (Figure 2f). Combining the corresponding SAED pattern (inset in Figure 2f), it can be concluded that exposed crystal plane of the c-CuO porous nanosheets is (110) planes. These SEM, TEM and HRTEM images demonstrated that a-CuO and c-CuO porous nanosheets have been successfully prepared, respectively.

In order to explain the formation mechanism of the pores, the thermal behaviours of $Cu_2(OH)_2CO_3$ were carried out by thermo-gravimetric analysis (TGA). The result shows that the reason for pore formation of CuO samples was due to the thermal decomposition of the precursor (Figure S5). N_2 adsorption-desorption analysis demonstrate that the Brunauer-Emmett-Teller (BET) surface area of a-CuO and c-CuO was 18.9 m^2/g and 21.3 m^2/g, respectively, and their corresponding pore sizes were about 25 nm and 26 nm (Figure S6). Therefore, based on the above information, it can be seen that we have successfully prepared porous CuO nanosheets with different crystallinity, but having the almost same surface area, morphology and pore size, which provides appropriate samples for the comparative study of the gas sensitivity of amorphous and crystalline materials.

2.3. Gas Sensing Properties of c-CuO Porous Nanosheets

Firstly, the gas sensing properties of c-CuO porous nanosheets were investigated systematically. It is generally known that the sensitivity of the gas sensor is directly affected by operating temperature, therefore, a series of experiments were used to determine the best operating temperature of c-CuO-based gas sensor. As shown in Figure 3a, within the range of 100–440 °C, the gas responses have an obvious change. The sensitivity of the gas sensor increased from 100 °C to 260 °C and then decreased with the increase of operating temperature. Obviously, the sensitivity reached its maximum at 260 °C. This phenomenon is mainly because the lower working temperature restricts the adsorption of gases to be measured, it causes the reactions to be inadequate. On the contrary, the higher operating temperature greatly enhanced the desorption rate of gas molecules, which also affected the gas sensitivities.

The sensitivities to 100 ppm of n-butanol, acetone, alcohol, methanal and methyl alcohol were shown in Figure 3b, we can see that the sensor has obvious response to the common VOCs, and the sensitivity values for n-butanol, acetone, alcohol, methanal and methyl alcohol are 14.6, 5.9, 8.5, 10.5, and 4.1 respectively. Figure 3c shown that the c-CuO porous nanosheets have fast response and recovery ability at 260 °C to the VOCs. The response time to 100 ppm of n-butanol, acetone, alcohol, methanal and methyl alcohol were calculated to be 3, 12, 10, 12 and 14 s, respectively, while the recovery time were

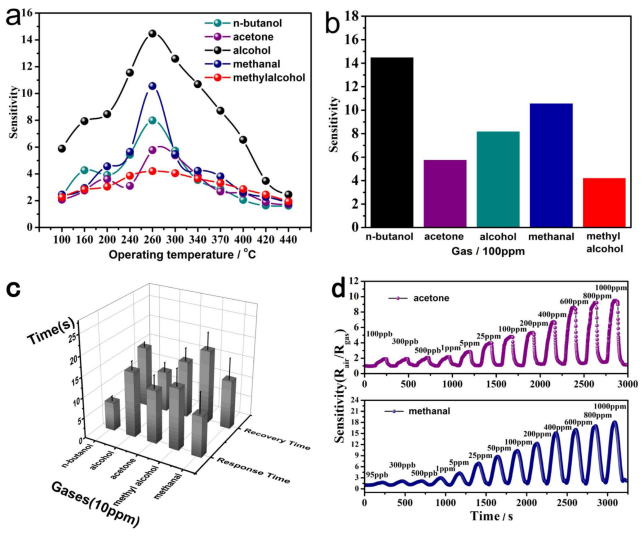

Figure 3. Gas sensing properties of c-CuO. (a) Best operating temperature of c-CuO porous nanosheets. (b) Gas sensing sensitivities of c-CuO porous nanosheets to 100 ppm of n-butanol, acetone, alcohol, methanal and methyl alcohol at 260 °C. (c) Response and recovery time of c-CuO porous nanosheets to corresponding VOC gases. (d) Real-time response of the c-CuO porous nanosheets to different concentrations of methanal and acetone at 260 °C.

calculated to be 4, 22, 4, 6 and 11 s, respectively. None of them exceeded 25 s. The continuous real-time responses of the c-CuO porous nanosheet-based sensor to different concentrations of methanal and acetone were presented in Figure 3d. It can be observed that the sensitivities to methanal and acetone changed significantly with the change of concentration. It not only exhibited good ability of continuous detection, but also showed good restorability to reach the initial value after each test cycle. It is necessary to mentioned that the lowest detection limits to methanal and acetone are both about 100 ppb. Refer to the international standards for indoor air quality (IAQ), the maximal allowable concentration of methanal is 60 ppb, obviously, the gas sensing activity of the c-CuO porous nanosheets can not meet the requirements of international standards.

2.4. Gas Sensing Properties of a-CuO Porous Nanosheets

As shown in Figure 4a, compared with the c-CuO porous nanosheets, the a-CuO porous nanosheets displayes greatly enhanced sensitivity to VOCs. When the gas concentration of alcohol, acetone and methyl alcohol was 50 ppm, the sensitivity of a-CuO is 8.9, 6.3, 7.5 times as high as that of the c-CuO, respectively. It is worth emphasizing specially that the enhancement factor of methanal was 11.2. At the same time, the a-CuO porous nanosheets clearly perform faster in response and recovery time compared with c-CuO porous nanosheets (Figure 4b), which about shortens 70–30% depending on the gas types. Even for the ultralow concentration of VOC samples (such as 60–10 ppb of methanal), these a-CuO porous nanosheets still exhibit excellent sensing activity with sensitivity resolution of 3.0 and 1.3. Such a high detection limit can fully meet the standards for formaldehyde detection requirements (Figure 4c).

The linearity at low gas concentration is also an important indicator of the sensing properties. In practice, it will be helpful to quantitatively determine the concentration of leaked gas. From Figure 4d, it can be seen that a-CuO and c-CuO porous nanosheets all show the excellent linear relation between concentration and sensitivity for the gases to be measured. Consequently, according to above-mentioned characterization results, it have been clearly demonstrated that the a-CuO porous nanosheets has better gas-sensing activities than c-CuO porous nanosheets.

Repeated experiments were carried out to verify the stability of the a-CuO porous nanosheets in the actual usage. It can be found that the sensitivity to methanal was kept constant in 100 test cycles (Figure 5a) and it presented nearly invariable response in the following 120 days, which suggests that it could can supply longer service life (Figure 5b). Besides these two tests, the resistance of gas sensor in the circuit stability was also studied. As is shown in Figure 5c, the U-I plots displayed the voltage of the sensor linearly depend on the current, so the component has a fixed resistance value whether in dark or under visible light environment, which also helps to provide accurate testing data to avoid misinformation. Moreover, SEM and TEM photos showed that the morphology and structure of the samples did not change significantly after repeated experiments (Figure S7).

2.5. Investigation of Gas Sensitivity Enhancement Mechanism

Several studies have confirmed that the sensing performance has a direct correlation with the structure and specific surface

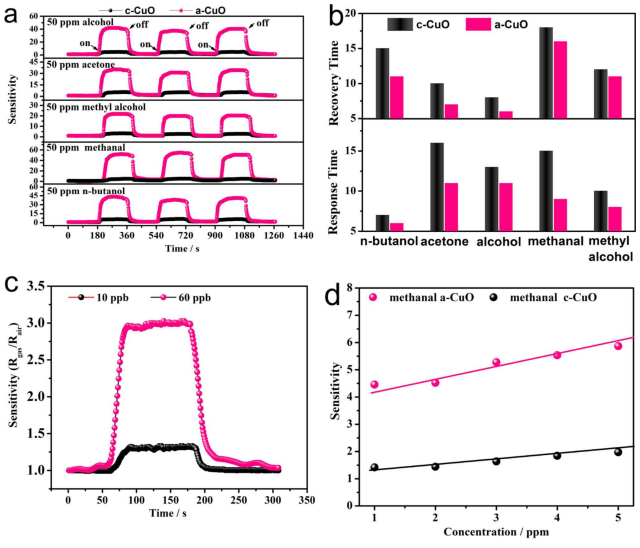

Figure 4. The comparison of gas sensitivity properties of a-CuO and c-CuO porous nanosheets: (a) The gas sensing sensitivity to 50 ppm alcohol, acetone, methyl alcoholand methanal at 260 °C. (b) Response and recovery time to different VOC gases. (c) The sensitivity of a-CuO porous nanosheets to 60 and 10 ppb methanal. (d) The linearities to 0.01–0.05 ppm methanal and methyl alcohol at 260 °C.

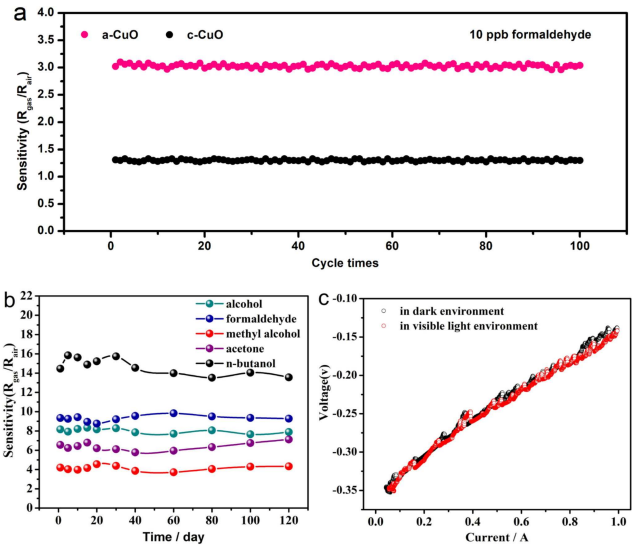

Figure 5. (a) a-CuO and c-CuO porous nanosheets show cyclic stability of sensitivity for low concentration methanal samples. (b) a-CuO porous nanosheets show a long-term stability of sensitivity for different VOCs. (c) The U-I plots displayed the voltage of the a-CuO porous nanosheets linearly depend on the current.

area.[28–30] In the present study, the high sensitivity and fast response-recovery time of a-CuO and c-CuO porous nanosheets can attributed to the help of their hierarchical and porous structure, which can provide larger specific surface area and form more gas channels, which enhance the utilization ratio of materials and offer much active sites to accelerate the rate of physical and chemical reaction.

Although both a-CuO and c-CuO porous nanosheets all show excellent gas sensitivity, it is obvious that a-CuO porous nanosheets is an order of magnitude more sensitive than c-CuO porous nanosheets. In order to explain the performance enhancements from the material itself, the electron spin resonance spectra (ESR) and X-ray photoelectron spectroscopy (XPS) of the a-CuO and c-CuO porous nanosheets were studied. ESR spectrum can accurately detect the information of unpaired electrons.[31] As shown in Figure 6a, these a-CuO porous nanosheets displayed a distinct single-electron signal with a g value at 2.03. Such strong single-electron signal undoubtedly proves that these porous a-CuO nanosheets contain high concentration of Vo defects.[32,33] In contrast, the ESR spectrum of c-CuO porous nanosheets shows no obvious single-electron signal, showing very high crystallinity. XPS spectra also show that these porous a-CuO nanosheets contain a large number of Vo defects. As shown in Figure 6b, Cu2p spectrum shows that these porous a-CuO nanosheets contain not only Cu^{2+} ions, but also a large number of Cu+ ions. The existence of Cu^{+} ions

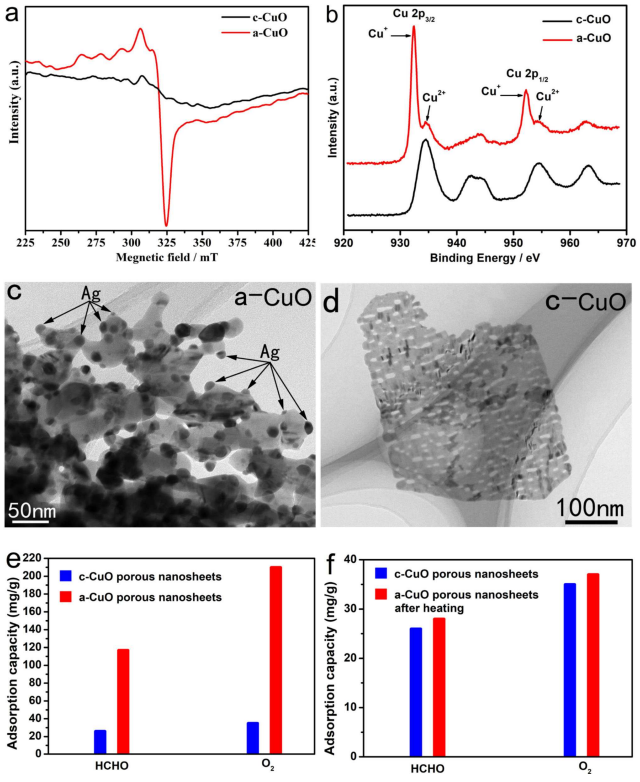

Figure 6. Characterization of surface properties of the a-CuO and c-CuO porous nanosheets. (a) ESR spectra. (b) XPS spectra. (c–d) TEM images obtained after the a-CuO and c-CuO porous nanosheets reacted with AgNO3 at room temperature. (e–f) The adsorption capacity of HCHO and O2 on a-CuO and c-CuO porous nanosheets.

once again confirms the existence of Vo defects in the porous a-CuO porous nanosheets. At the same time, because of the surface reducibility caused by the presence of a large number of Vo defects, these a-CuO porous nanosheets can in-situ reduce Ag^{+} ions to metal Ag nanoparticles without external reductants (Figure 6c and Figure S8). While for c-CuO porous nanosheets, there is no such phenomenon (Figure 6d). These results suggest that the presence of Vo-defects greatly improves the surface chemical activity of the a-CuO porous nanosheets.

The existence of these Vo-defects greatly improves the adsorption of methanal and oxygen molecules on the surface of the porous a-CuO nanosheets. Chemical adsorption experiments showed that the amount of methanal adsorbed by a-CuO nanosheets was 4.5 times higher than that by c-CuO nanosheets (Figure 6e). At the same time, the chemisorption capacity of a-CuO to O_2 is 32.6 times that of c-CuO to O_2. In addition, controlled experiments show that once these copper oxides are heated in the air to lose Cu^{+} ions and the corresponding Vo-defects, their adsorption capacity to methanal and oxygen molecules tends to be the same (Figure 6f). Considering that the morphology, specific surface area and particle size of the a-CuO nanosheets and the c-CuO nanosheets are basically the same, the huge difference in methanal and adsorption may be rationally attributed to the difference of Vo-defect concentration between a-CuO and the c-CuO.

In order to further clarify the underlying mechanism for the higher gas-sensing activity of a-CuO porous nanosheets relative to c-CuO porous nanosheets, we further studied the methanal and oxygen adsorption structures and energies on the porous a-CuO and c-CuO nanosheets through density functional theory (DFT) calculations. On the one hand, as show in Figure 7a, methanal is weakly physisorbed over the perfect c-CuO nanosheets, with low adsorption energy of −0.096 eV and no strong preference for a particular surface site. When a large number of oxygen vacancies are created on the surface and inside of the porous a-CuO nanosheets, Cu+ ions are exposed, which leads to a much stronger adsorption of methanal molecules through O at the defect site of the porous a-CuO nanosheets (Figure 7b). The calculated adsorption energy for methanal molecules is up to −0.257 eV. On the other hand, for oxygen molecules, the difference in adsorption energy is more obvious. As shown in Figure 7c-d, the adsorption energy of O_2 on the (110) face of c-CuO porous nanosheets is only −0.019 ev, while that is −1.199 ev for a-CuO porous nanosheets, almost 63 times the difference. It is well known that methanal and oxygen molecules will arise redox reaction on the surface of gas sensitive materials, resulting in sensing properties (changes in resistivity of sensitive materials), therefore, combining the results of these experiments and theoretical calculations, the improvement of gas sensing property can be reasonably attributed to the increase of adsorption energy caused by high concentration oxygen vacancy defects contained in the a-CuO porous nanosheets.

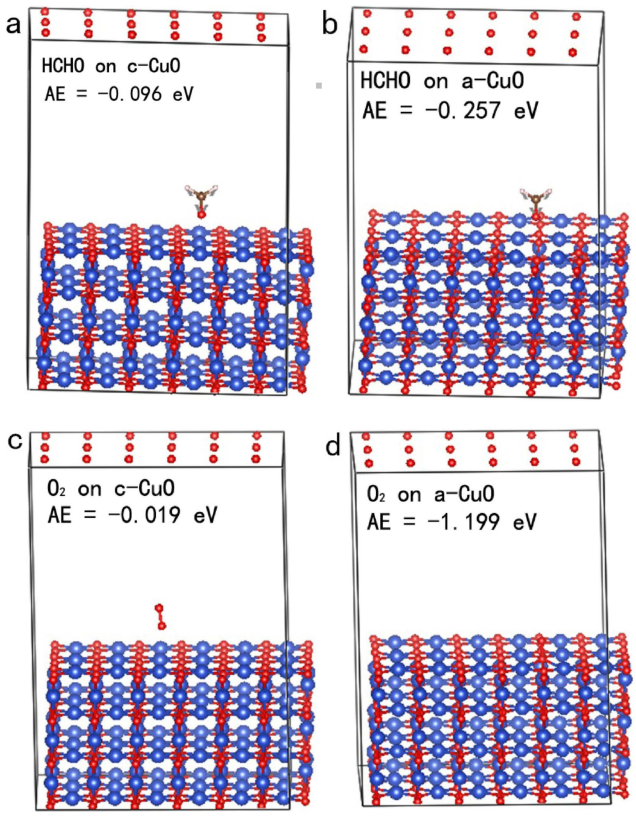

Figure 7. Calculation of adsorption energy (AE) of methanal and oxygen molecules on (a,c) c-CuO and (b,d) a-CuO porous nanosheets.

3. Conclusions

In summary, hierarchical porous CuO microspheres with amorphous porous nanosheets were successfully synthesized by a very simple and rapid microwave heating method. Compared with crystalline CuO porous nanosheets, the amorphous CuO porous nanosheets contain a large number of oxygen vacancies, which lead them to possess much strong adsorption for methanal and oxygen. As a new gas-sensing material, the oxygen vacancy-rich and amorphous CuO porous nanosheets show an unexpected remarkable sensitivity to a series of VOCs containing oxygen groups such as methanal. This work presents not only a possibility for the fabrication of amorphous CuO porous nanosheets as an efficient gas sensor but also offer an important concept that Vo-rich amorphous simple oxides can be used as a new strategy to design materials with high gas-sensing activity.

Experimental Section

Synthesis of Hierarchical Porous c-CuO Microspheres Composed of Porous Nanosheets

The crystalline c-CuO porous nanosheet microspheres could be acquired by annealing the $Cu_2(OH)_2CO_3$ precursors from room temperature to 400 °C raised at a speed 1 °C min−1 and kept at 400 °C for 2 h. After that, the obtained products were washed 2 times with deionizer water and absolute ethanol respectively, and collected by centrifugation and dried at 50 °C for 1 h.

Synthesis of Hierarchical Porous a-CuO Microspheres Composed of Porous Nanosheets

In a typical synthesis, 0.5 g of $Cu_2(OH)_2CO_3$ powders were dispersed in 30 mL of ultrapure water by ultrasonic oscillation. The obtained suspension solution was heated for 5 minutes by microwave with a power of 400 W. After collecting and washing the resulting black precipitate, the amorphous a-CuO could be obtained.

Gas Sensing Test

In the present experiments, we use the gas sensing measurement system (Winsen, WS-30 A) to research the gas sensing properties of crystalline c-CuO and amorphous a-CuO samples. The gas sensors chosen in the experiments belong to indirectly heated type. In the process of constructing gas sensitive elements, appropriate amount of a-CuO or c-CuO powders were ground in a mortar with dropping a few drops of alcohol to serve as sensitive material layer. After that, the sensitive material was coated on the surface of the alumina ceramic tube to make sure the two Au electrodes and four Pt wires were completely covered. Then, the Ni–Cr alloy wire was inserted into the ceramic tube to provide heating temperature which could be controlled by adjusting the test voltage. Eventually, the gas sensors were aged for 1 day at 200 °C in air to improve the stability and service life. The structure and circuit diagram of the gas sensor are shown in Figure S1. In order to reduce the impact of external environmental factors, in each gas sensing properties test, the relative humidity were all maintained at around 25 %. The calculation of sensitivity, response and recovery time is displayed in the Supporting Information.

Acknowledgements

This work received financial support from the Science Foundation of Chinese Academy of Inspection and Quarantine (2019JK004) and the National Key Research and Development Program of China (2017YFF0210003).

Keywords: porous nanosheets · amorphous nanostructures · gas-sensing · adsorption energy · oxygen vacancies

[1] H. W. Lin, M. Jang, K. S. Suslick, *J. Am. Chem. Soc.* **2011**, *133*, 16786–16789.
[2] S. Dolai, S. K. Bhunia, S. S. Beglaryan, S. Kolusheva, L. Zeiri, R. Jelinek, *ACS Appl. Mater. Interfaces* **2017**, *9*, 2891–2898.
[3] J. Guo, Y. Jiang, X. F. Hu, Z. M. Xu, *Environ. Sci. Technol.* **2012**, *46*, 1028–1035.
[4] J. N. Fu, L. N. Zhang, *Anal. Chem.* **2018**, *90*, 8080–8090.
[5] L. Feng, C. J. Musto, K. S. Suslick, *J. Am. Chem. Soc.* **2010**, *132*, 4046–4047.
[6] R. J. Hopkinson, C. J. Schofield, *Biochemistry* **2018**, *57*, 904–910.
[7] R. Ab Kadir, R. Abdul Rani, M. M. Y. A. Alsaif, J. Z. Ou, W. Wlodarski, A. P. O'Mullane, K. Kalantar-zadeh, *ACS Appl. Mater. Interfaces* **2015**, *7*, 4751–4757.
[8] L. G. Bloor, J. Manzi, R. Binions, I. P. Parkin, D. Pugh, A. Afonja, C. S. Blackman, S. Sathasivam, C. J. Carmalt, *Chem. Mater.* **2012**, *24*, 2864–2866.
[9] L. Li, S. J. He, M. M. Liu, C. M. Zhang, W. Chen, *Anal. Chem.* **2015**, *87*, 1638–1645.

[10] W. T. Koo, S. J. Choi, S. J. Kim, J. S. Jang, H. L. Tuller, I. D. Kim, *J. Am. Chem. Soc.* **2016**, *138*, 13431–13437.
[11] Y. L. Wang, X. C. Jiang, Y. N. Xia, *J. Am. Chem. Soc.* **2003**, *125*, 16176–16177.
[12] X. X. Xu, J. Zhuang, X. Wang, *J. Am. Chem. Soc.* **2008**, *130*, 12527–12535.
[13] D. S. Dhawale, T. P. Gujar, C. D. Lokhande, *Anal. Chem.* **2017**, *89*, 8531–8536.
[14] X. Z. Wang, W. Liu, J. R. Liu, F. L. Wang, J. Kong, S. Qiu, C. Z. He, L. Q. Luan, *ACS Appl. Mater. Interfaces* **2012**, *4*, 817–820.
[15] Z. G. Xie, L. Q. Ma, K. E. deKrafft, A. Jin, W. B. Lin, *J. Am. Chem. Soc.* **2010**, *132*, 922–923.
[16] P. C. Xu, H. T. Yu, X. X. Li, *Anal. Chem.* **2011**, *83*, 3448–3450.
[17] J. Shu, Z. L. Qiu, S. Z. Lv, K. Y. Zhang, D. P. Tang, *Anal. Chem.* **2017**, *89*, 11135–11142.
[18] J. Su, X. X. Zou, Y. C. Zou, G. D. Li, P. P. Wang, J. S. Chen, *Inorg. Chem.* **2013**, *52*, 5924–5930.
[19] L. Z. Zhang, Q. L. Fang, Y. H. Huang, K. W. P. K. Xu, Chu, F. Ma, *Anal. Chem.* **2018**, *90*, 9821–9822.
[20] B. Tong, Z. H. Deng, B. Xu, G. Meng, G. Z. Shao, H. Y. Liu, T. T. Dai, X. Y. Shan, W. W. Dong, S. M. Wang, S. Zhou, R. H. Tao, X. D. Fang, *ACS Appl. Mater. Interfaces* **2018**, *10*, 34727–34730.
[21] S. Steinhauer, A. Chapelle, P. Menini, M. S. Local, *ACS Sens.* **2016**, *1*, 503–504.
[22] A. Taubert, F. Stange, Z. H. Li, M. Junginger, C. Günter, M. Neumann, A. Friedrich, *ACS Appl. Mater. Interfaces* **2012**, *4*, 791–795.
[23] X. Liu, B. S. Du, Y. Sun, M. Yu, Y. Q. Yin, W. Tang, C. Chen, L. Sun, B. Yang, W. W. Cao, M. N. R. Ashfold, *ACS Appl. Mater. Interfaces* **2016**, *8*, 16379–16380.
[24] M. Shafiei, F. Hoshyargar, J. Lipton-Duffin, C. Piloto, N. Motta, A. P. O'Mullane, *J. Phys. Chem. C* **2015**, *119*, 22208–22216.
[25] G. X. Zhu, H. Xu, Y. Y. Xiao, Y. J. Liu, A. Yuan, X. P. Shen, *ACS Appl. Mater. Interfaces* **2012**, *4*, 744–750.
[26] Y. P. Wu, W. Zhou, W. W. Dong, J. Zhao, X. Q. Qiao, D. F. Hou, D. S. Li, Q. C. Zhang, P. Y. Feng, *Cryst. Growth Des.* **2017**, *17*, 2158–2262.
[27] Y. Qin, F. Zhang, Y. Chen, Y. J. Zhou, J. Li, A. W. Zhu, Y. P. Luo, Y. Tian, J. H. Yang, *J. Phys. Chem. C* **2012**, *116*, 11994–12000.
[28] A. Kaushik, R. Kumar, S. K. Arya, M. Nair, B. D. Malhotra, S. Bhansali, *Chem. Rev.* **2015**, *115*, 4571–4606.
[29] J. Bai, B. X. Zhou, *Chem. Rev.* **2014**, *114*, 10131–10176.
[30] H. K. Wang, A. L. Rogach, *Chem. Mater.* **2014**, *26*, 123–133.
[31] H. Bai, W. C. Yi, J. F. Li, G. C. Xi, Y. H. Li, H. F. Yang, J. Y. Liu, *J. Mater. Chem. A* **2016**, *4*, 1566–1670.
[32] Z. Li, C. Xiao, H. Zhu, Y. Xie, *J. Am. Chem. Soc.* **2016**, *138*, 14810–14825.
[33] F. C. Lei, Y. F. Sun, K. T. Liu, S. Gao, L. Liang, B. C. Pan, Y. Xie, *J. Am. Chem. Soc.* **2014**, *136*, 6826–683

Manuscript received: November 4, 2019
Revised manuscript received: December 20, 2019
Accepted: ■■, ■■■